

Frequency Stability Control in Low-Inertia Microgrids Using Optimized Virtual Damping Stabilizers

Sabo Aliyu *^{id}, I. Dabo Abdulmalik *^{id}, Dauda Dahiru *^{†id}, Kabiru Abubakar Tureta *^{id}
Kenneth Okedu **^{†id}, Noor Izri Abdulwahab ***^{id}

* Department of Electrical Engineering, Faculty of Engineering and Engineering Technology, Nigerian Defense Academy, Kaduna, Nigeria.

** School of Information Technology and Engineering, Melbourne Institute of Technology, 3000, Victoria, Australia.

*** Department of Electrical and Electronic Engineering, Faculty of Engineering, University Putra Malaysia.

(saboaliyu98@gmail.com, abdulmalikdabo@gmail.com, dawooddahiru@gmail.com, kabiruabubakartureta@gmail.com, kokedu@academic.mit.edu.au, izzri@upm.edu.my)

[†]Corresponding Authors: Kenneth Okedu and Dauda Dahiru, kokedu@academic.mit.edu.au and dawooddahiru@gmail.com.

Received: 09.02.2026, Revised: 07.03.2026, Accepted: 08.03.2026

Abstract- Inverter-based Generators generally lack natural inertia required for ascertaining the frequency stability of Electrical Microgrid Power Systems. A robust virtual inertia emulation technique is required in ensuring that frequency stability of low-inertia systems is greatly improved. This paper presents a hybrid control strategy that combines Fractional Derivative Inertia Control (FDIC) and a Virtual Damping Stabilizer (VDS) modelled as lead-lag compensator, and then as FOPID, implemented via a Battery Energy Storage System (BESS) to address these challenges. The FDIC is a BESS-based virtual inertia controller that leverages fractional calculus to emulate inertia and damping, while the VDS generates the appropriate compensating power that helps dampen out oscillations. A comprehensive MATLAB/Simulink model of an islanded microgrid comprising a diesel generator, photovoltaic (PV), and wind generation is developed to evaluate the proposed approach. Control parameters are optimized using the Beluga Whale Optimization Algorithm (BWO), ensuring robust performance under various disturbances and its performance is evaluated by comparison with Particle Swarm Optimization (PSO) based VDS design. Simulation results demonstrate that the FDIC+VDS scheme significantly improves frequency deviation compared to traditional virtual inertia. The findings highlight the efficacy of advanced BESS-based control strategies in enhancing the resilience and stability of low-inertia, renewable-rich microgrids.

Keywords: Microgrid, frequency control, virtual damping stabiliser, FOPID, FDIC.

1. Introduction

The transition towards sustainable and low-carbon energy systems has driven a rapid proliferation of renewable energy

sources (RES) such as photovoltaic (PV) and wind energy in power systems. Islanded microgrids, often deployed in remote or off-grid areas, have become a practical platform for integrating these intermittent energy sources due to their

ability to operate independently of the main grid. However, the high penetration of inverter-based RES introduces significant technical challenges, primarily due to the lack of inherent inertia [1, 2, 3] and damping typically provided by synchronous generators. This deficiency leads to frequency instability, degraded power quality, and a general decline in system resilience under disturbances. Microgrid control is essential, because it helps keep the system stable. . Microgrid control strategies are mainly of two types, Primary/Secondary control and peer-to-peer control [4]. The prime control perspectives in the MG based on Primary/Secondary control are: voltage, current, frequency, proper power-sharing active, and reactive [5, 6, 7]. Droop control is a common control strategy in peer-to-peer control which uses real power output from a generator to calculate the operating frequency and offset the effect of fast changing loads [8]. Droop control involves controlling voltage droop or frequency droop. When multiple micro-sources engage in providing power balance, they will follow either the voltage droop or the frequency droop method [9]. This control level aims to maintain output voltage regulation and active power [10, 11, 12, 13]. In conventional grid-tied systems, rotational inertia and power system stabilizers (PSS) inherently mitigate frequency deviations and oscillations following load or generation disturbances [14]. However, in islanded microgrids dominated by power-electronics-based generation, these stabilizing mechanisms are either absent or significantly reduced [15]. Consequently, the dynamic performance of such systems becomes highly sensitive, especially during events such as load changes, RES intermittency, and faults [16, 17, 18]. The limited availability of primary frequency control and insufficient damping necessitate the design of advanced control strategies capable of emulating the stabilizing effects of conventional generators.

Virtual inertia control is a control technique that was first developed using the derivative control technique to mimic the inertia offered by the rotating mass of synchronous generators (SG) but neglected the damping properties. Authors in [19] introduced fractional derivative virtual inertia integrated into the virtual inertia control loop to address microgrid (MG) stability issues. Though it was an improvement on the derivative technique, but it also neglected the damping properties. Subsequent studies like that of [20, 2] have proved that the virtual inertia control incorporated with the virtual damping has a better frequency response than the virtual inertia control based on derivative inertia control (DIC) technique regarding damping frequency oscillation and shortening the settling time.

Over the years, researchers have proposed various control methods to reduce frequency deviations and enhance system stability. The authors in [21] propose a self-tuning PI-controller that utilizes a combination of Artificial Neural Networks (ANN) and Genetic Algorithms (GA), which enables online training and adjustment of the PI-controller coefficients. The proposed method showed improved performance in terms of frequency stability, with reduced fluctuations in the microgrid's frequency response compared to traditional methods. While the proposed method enhanced the stability and performance of the microgrid, the integration

of ANN and GA introduces computational complexity that may not be manageable with standard processing units. The authors acknowledge that high-resolution processors are necessary to handle the extensive calculations involved, which can increase the overall cost and complexity of the control system. In another study, [22] proposed a Decentralized utilization of distributed energy storage resources for simultaneous frequency regulation in a microgrid. Wind and PV generation systems were combined for the enhancement of inertia and frequency support. The result showed that using PV only, wind only, or simultaneously using both enhanced the frequency deviation by 44.4 %, 29.5 % and 53.3 % respectively. In addition, the required energy from PV and wind using both simultaneously, is reduced by 29.5 % and 13.7 % and ROCOF is enhanced by 61.9 %. While the proposed method proved effective, the effectiveness of the proposed control scheme is inherently tied to the availability of sunlight and wind. Variability in these renewable resources can lead to inconsistent performance, particularly during periods of low generation, which may not be adequately addressed in the proposed strategy. Furthermore, [23] proposed a coordinated control parameter setting of DFIG wind farms with virtual inertia control by utilizing virtual inertia from wind farms to enhance the frequency stability of power systems. The propose method adjusts the active power output based on system frequency feedback which is significant as it mimics the behavior of synchronous generators, providing necessary inertia support in systems with low natural inertia. While the authors present a comprehensive approach, it could benefit from a more detailed comparison with existing methods to provide a clearer context for the advantages of the proposed approach. In [24], the authors presented a frequency control method that utilizes electric spring (ES) technology to provide virtual inertia and primary frequency response through smart loads (SL). The ES technology allows voltage-dependent loads to operate as smart loads, which can modulate their power consumption within a specified voltage range ($\pm 5\%$ of nominal voltage). The control design allowed the system to provide up to 2.5 seconds of virtual inertia under specific conditions. The system frequency nadir improved from 48.95 Hz to 49.3 Hz when the smart load was active. While the frequency nadir improved, the practical implementation challenges, such as the integration of electric spring (ES) technology into existing infrastructure and the economic feasibility of widespread adoption, are not thoroughly addressed. In [25] a Variable Synthetic Inertia Controller for Wind Turbine Generators was presented as an innovative frequency control method through the design and implementation of a Variable Hidden Inertia Emulator (VHIE) for Wind Turbine Generators (WTGs) equipped with Permanent Magnet Synchronous Generators (PMSGs). The initial tests were conducted on a simplified configuration, followed by more realistic simulation. The simulations demonstrated that the VHIE controller effectively reduced the Rate of Change of Frequency (RoCoF) by approximately 40%. The frequency nadir, which is the lowest point of frequency during a transient, showed a 35% improvement. Although the VHIE aims to provide effective frequency support, its performance during rapid frequency transients may still be limited. The synthetic inertia

coefficient's dependence on rotor speed means that during critical moments of frequency deviation, the controller's effectiveness could diminish, potentially leading to inadequate support when it is most needed.

Furthermore, [26] proposed an innovative frequency control method known as Adaptive Optimal Model Predictive Control (AOMPC). The AOMPC method was compared with various existing controllers, including optimal proportional-integral (OPI), optimal fractional order PID (OFOPID), optimal fuzzy PID (OFPID), and adaptive MPC (AMPC). The results indicated that AOMPC provided the best performance in terms of frequency regulation during multiple load disturbances and changes in weather patterns. Although the AOMPC proved to be better than the compared controllers, the implementation of AOMPC may involve complex computations and require advanced algorithms, such as the CPSO algorithm for parameter tuning. This complexity could pose challenges in real-time applications, especially in systems with limited computational resources.

In [27], the authors presented a virtual inertia control-based vehicle-to-grid (V2G) concept for the secondary load frequency control of AC islanded microgrids (MGs). The proposed control approach outperforms conventional MPC (CMPC) and model-free Sliding Mode Control (MFSMC) in terms of frequency regulation. The stored energy in electric vehicles was effectively utilized to enhance both steady-state and transient performance, showcasing the benefits of integrating V2G technology into frequency control strategies. The study assumes that electric vehicles can be effectively controlled as mobile energy storage devices. However, this assumption may not hold true in all cases, as user behavior, charging patterns, and vehicle availability can vary significantly. These factors could impact the reliability of the V2G system and its ability to provide the necessary virtual inertia.

In another study, [28] proposed a frequency control method that combines virtual inertia and damping, optimized through genetic algorithms. The proposed VI control system not only enhances the dynamic response and frequency regulation of the microgrid but also demonstrates robustness against various operational challenges. The study relies heavily on Genetic Algorithm (GA) for optimizing the parameters of the VI control system. While GA is known for its fast convergence, the study does not explore alternative optimization methods or provide a comparative analysis of their effectiveness.

In [29], the authors proposed a frequency control method which is an adaptive virtual inertia control method. The adaptive virtual inertia control led to a marked improvement in frequency response, minimizing frequency deviations and enhancing overall system stability. The proposed method-maintained effectiveness even with communication delays of up to 100ms, ensuring continued performance in large networks. While the proposed control method shows promise, the control strategy relies heavily on distributed communication among VSG units. This dependency can introduce vulnerabilities if communication is disrupted.

The authors in [30] proposed a virtual inertia emulator (VIE) based Model predictive control MPC as a frequency control method. The MPC approach can reduce the minimum Energy Storage System (ESS) capacity required for frequency regulation by 55% compared to a P controller and by 2% compared to a PI controller. The energy throughput of the ESS using MPC was found to be reduced by 86% compared to a P controller and by 36% compared to a PI controller. The study emphasizes that MPC effectively minimizes frequency deviation during disturbances, showcasing its superior performance over traditional control methods. While the authors claim that the MPC can operate in real-time due to its one-step prediction horizon, the computational demands of MPC can still be significant, especially in larger and more complex systems.

In [31], the authors proposed a virtual inertia control based on proportional-integral (PI) controller optimally designed by the Manta Ray Foraging Optimization (MRFO) as a frequency control method. The study investigates the microgrid's performance under step load changes, specifically highlighting a 50% reduction in overall inertia. Although the MRFO-based PI controller demonstrated improved system performance in frequency disturbance alleviation and reference frequency tracking, the results indicate significant frequency fluctuations and deviations during these disturbances, suggesting that there is a clear need for more advanced control mechanisms that can provide better damping and stability. Virtual damping stabilizers, for instance, could offer a more robust solution by improving system response to disturbances and sudden load change.

This study proposes an enhanced frequency control scheme combining Fractional Derivative Inertia Control (FDIC) and a Virtual Damping Stabilizer (VDS) integrated through a Battery Energy Storage System (BESS). The FDIC extends traditional virtual inertia concepts by incorporating fractional calculus to provide a more flexible and accurate dynamic response, which better mimics the non-local and history-dependent nature of real physical inertia. This approach allows for tunable control dynamics that adapt to varying system conditions, resulting in improved frequency nadir, settling time, and overshoot performance.

Simultaneously, the VDS complements the inertia emulation by providing synthetic damping through active power modulation. The BESS acts as the physical actuator, delivering rapid response capabilities essential for dynamic support in inverter-based systems. Together, the FDIC and VDS form a coordinated control framework aimed at stabilizing frequency oscillations and improving system damping without the need for mechanical inertia.

This work contributes the following key innovations:

- Development of a hybrid FDIC-VDS scheme that combines the benefits of fractional order dynamics with fast-acting synthetic damping control.
- Modelling of VDS in two different configurations: VDS modelled as a lead-lag compensator, then as FOPID for performance evaluation.

- Integration of BESS for dynamic support, acting as both inertia emulator and damping stabilizer within a unified control architecture.
- Optimization and tuning of control parameters using Beluga Whale optimizer (BWO), a nature-inspired algorithm to enhance system performance across a range of operating conditions.

The system is modelled and simulated in MATLAB/Simulink, where the dynamic interactions between the diesel generator, renewable energy sources, and BESS-based control mechanisms are comprehensively evaluated. The performance of the proposed control strategy is benchmarked against conventional virtual inertia and droop control methods, demonstrating superior frequency stability, reduced oscillations, and enhanced robustness to disturbances. The proposed control strategy is also modelled in two different architectures: as a lead-lag compensator and as FOPID, with the FOPID configuration showing better overall performance.

1.1. Problem Statement

The increasing integration of renewable energy sources (RESs) into microgrids has led to a significant reduction in system inertia, resulting in instability issues during frequency disturbances. Inverter-based generators lack natural inertia, which exacerbates frequency fluctuations and can lead to severe operational challenges in maintaining system stability. Another advantage offered by synchronous generator-based systems is the incorporation of Power system stabilizers (PSS) which is absent in inverter-based systems. The low capacity of BESS restricts their ability to respond effectively to frequency disturbances. Addressing this limitation with larger energy storage will significantly increase the initial investment cost.

2. System Modelling

The proposed study models an islanded microgrid with high renewable energy penetration, integrating a diesel

generator (DG), photovoltaic (PV) arrays, a wind turbine generator (WTG), and a Battery Energy Storage System (BESS) controlled via a hybrid Fractional Derivative Inertia Control (FDIC) and Virtual Damping Stabilizer (VDS) schemes. All disturbances were introduced as step inputs applied at $t = 15$ s, representing sudden changes in load demand or renewable generation. These are represented by the disturbance vector $u = [\Delta P_{LOAD}, \Delta P_{WIND}, \Delta P_{SUN}]^T$, applied to the microgrid state-space model to assess system resilience. This simplification isolates the transient response of the microgrid frequency control mechanism without stochastic weather dynamics. The magnitude of the step was normalized to $\pm 20\%$ for load and $\pm 10\%$ for renewable generation. The model is developed in MATLAB/Simulink, capturing the dynamic behaviors of the microgrid under various operating conditions.

2.1. Microgrid Architecture

The frequency dynamics of an islanded microgrid are critically influenced by the balance between generation and demand [32], especially in systems with high renewable energy penetration and limited rotational inertia. The schematic presented in Figure 1 shows the detailed frequency control architecture adopted for this study. The presented model offers a comprehensive dynamic frequency response framework that captures the contribution of both conventional and inverter-based resources (solar PV and wind) in regulating frequency deviation (Δf) following active power imbalances (ΔP).

Frequency stability during contingency events in the traditional power system is attributed to the PSS in SGs, damping winding, and inherited rotating mass inertia. The relationship between power imbalance, damping, frequency deviation, and system inertia is explained by the well-known swing equation in Equation 1.

$$\Delta P_m(s) + \Delta P_{Load}(s) = 2H_s \Delta F(s) + D \Delta F(s) \quad (1)$$

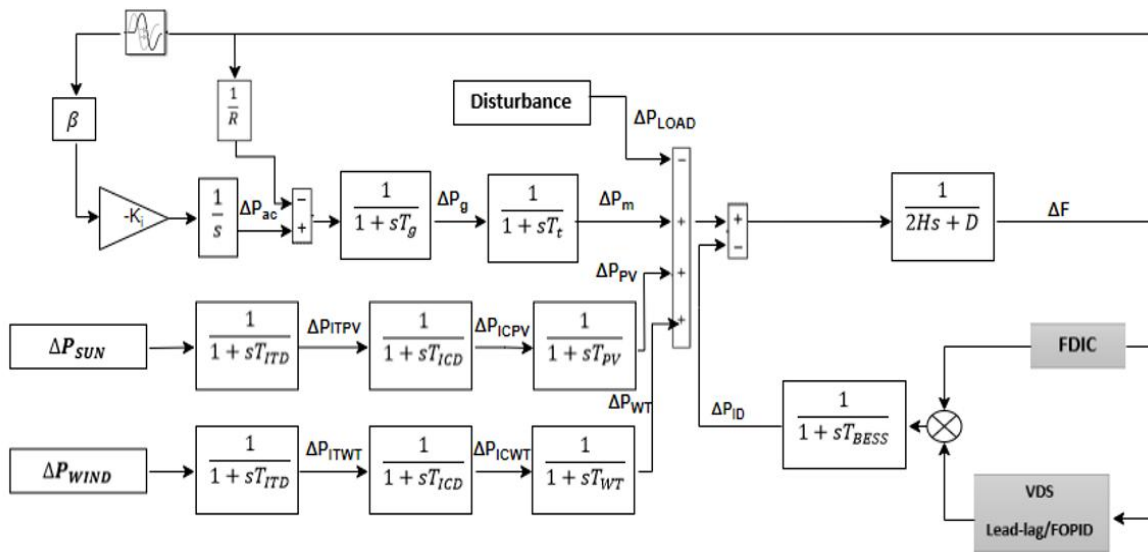


Fig. 1. Dynamic frequency response model of islanded microgrid.

Here, H represents the equivalent per-unit inertia constant of the microgrid, while D denotes the damping coefficient that captures the load-frequency sensitivity. The net power imbalance, defined as the deviation between total generation (including BESS compensation) and load demand, directly drives the frequency deviation Δf . The swing equation block thereby serves as the dynamic integrator translating power perturbations into frequency excursions. Therefore, the frequency deviation can be expressed from the model as:

$$\Delta F = \frac{(\Delta P_m + \Delta P_{PV} + \Delta P_{WT} - \Delta P_{ID} - \Delta P_{Load})}{2Hs + D} \quad (2)$$

The simulated islanded microgrid includes:

- A conventional diesel generator (DG), as the primary inertial component in the system, is modeled with detailed governor and turbine dynamics.
- Both photovoltaic (PV) and wind generation modeled using first-order transfer functions that reflect the dynamics of inverter-based control and active power injection.
- A BESS in augmenting the frequency stability of the microgrid by emulating both virtual inertia and virtual damping through injection/absorption of active power.
- A control loop implementing FDIC and VDS to emulate inertia and damping.

2.2. Diesel Generator Dynamics

The diesel generator is modeled using a second-order swing equation that captures the mechanical-electrical dynamics, including governor and turbine time constants. Its contribution to frequency regulation is also parameterized through droop control [33].

$$\Delta f = \frac{1}{2H} (\Delta P_m - \Delta P_g - D\Delta f) \quad (3)$$

where;

Δf : The rate of change of frequency deviation (ROCOF)-how quickly the frequency is changing over time due to imbalances in power.

H : The inertia constant of the machine (in seconds), representing stored rotational kinetic energy. A higher H implies more resistance to frequency change.

ΔP_m : The change in mechanical input power from the prime mover.

ΔP_g : The change in governor action.

Δf : The deviation in system frequency from the nominal value.

D : The damping coefficient, which models how the system naturally opposes frequency deviation (due to load-frequency sensitivity or artificial damping mechanisms).

The modeling of governor and turbine:

$$\Delta P_m = \frac{1}{1+sT_t} \Delta P_g \quad (4)$$

$$\Delta P_g = \frac{1}{1+sT_g} (\Delta P_{ac} - \Delta F \frac{1}{R}) \quad (5)$$

$$\Delta P_{ac} = -K_i \cdot \frac{1}{s} (\Delta F \beta) \quad (6)$$

Where; T_g and T_t are time constants of the governor and turbine of the diesel power plant respectively.

The generator output power ΔP_m is regulated through a proportional droop mechanism characterized by $\frac{1}{R}$, where R is the droop gain, and a supplementary integral controller with gain K_i .

The controller acts on the measured frequency deviation Δf , enhancing steady-state frequency restoration and robustness under disturbances. The integral action ensures zero steady-state error in frequency, particularly crucial in islanded settings where load-generation mismatches persist longer than in grid-connected modes. β is the frequency bias factor.

2.3. Renewable Energy Sources

PV and wind systems are modeled as inverter-based sources lacking physical inertia. Their generation profiles are subject to irradiance and wind speed variations, respectively. Their control is based on maximum power point tracking (MPPT) and active/reactive power control schemes [34]. Due to the inverter interface, these sources contribute negligible inertia, exacerbating frequency deviations during transients.

Modeling of photovoltaic (PV) power plants describes the generation system of solar energy. It can be expressed in a first-order transfer function.

$$\Delta P_{PV} = \frac{1}{1+sT_{PV}} \Delta P_{ICPV} \quad (7)$$

$$\Delta P_{ICPV} = \frac{1}{1+sT_{ICD}} \Delta P_{ITPV} \quad (8)$$

$$\Delta P_{ITPV} = \frac{1}{1+sT_{ITD}} \Delta P_{SUN} \quad (9)$$

ΔP_{SUN} is an external random disturbance and T_{PV} is the time constant of the PV power plant.

ΔP_{ITPV} and ΔP_{ICPV} are changes in solar PV power due to the inverter and interconnection time delay, respectively.

Modeling of wind power plants describes the generation system of wind energy. It can be expressed in a first order transfer function as shown in Equation 10 [35].

$$\Delta P_{WT} = \frac{1}{1+sT_{WT}} \Delta P_{ICWT} \quad (10)$$

$$\Delta P_{ICWT} = \frac{1}{1+sT_{ICD}} \Delta P_{ITWT} \quad (11)$$

$$\Delta P_{ITWT} = \frac{1}{1+sT_{ITD}} \Delta P_{WIND} \quad (12)$$

ΔP_{WIND} Is an external random disturbance. K_w and T_w are gain and time constant of the wind power plant.

ΔP_{ITWT} and ΔP_{ICWT} are changes in solar PV power due to the inverter and interconnection time delay, respectively.

2.4. Battery Energy Storage System (BESS)

To enhance microgrid frequency response and stability, the BESS-based inertia emulation control loops is required. The BESS is modeled as an ideal bidirectional power interface for short-term dynamic frequency control.

The model focuses on the dynamic frequency response behavior rather than energy management or SOC estimation. This assumption is consistent with previous inertia-emulation studies that use idealized storage dynamics to isolate control performance. These limits provide a physically consistent framework for short-term dynamic simulations without imposing energy saturation effects.

The simplified representation allows focus on the effectiveness of the FDIC-VDS coordination in stabilizing microgrid frequency during transient events. The transfer functions of the energy storage systems are given as shown in equation [35]:

$$\frac{1}{1+sT_{BESS}} \quad (13)$$

where, T_{BESS} is the time constant of battery energy storage system (BESS).

2.5. Fractional Derivative Inertia Control (FDIC)

The Fractional Derivative Inertia Control (FDIC) is a control strategy designed to emulate the inertial and damping behavior of conventional synchronous machines within converter-dominated microgrids using a Battery Energy Storage System (BESS).

Unlike classical integer-order control approaches, the FDIC employs fractional calculus, which allows for more flexible and accurate dynamic representation of inertia and damping effects.

As shown in Fig. 2, The FDIC generates a control signal ΔP_{FDIC} in response to a frequency deviation Δf . The signal is defined domain as:

$$\Delta P_{FDIC} = (H_{FDIC}S^\mu + D_{FDIC}) \Delta F \quad (14)$$

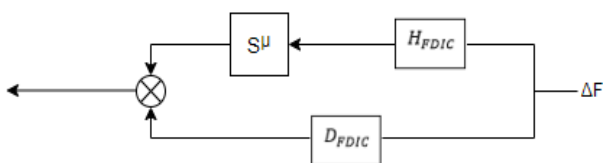


Fig. 2. FDIC control loop.

- ΔP_{FDIC} : The change in power contributed by the Fractional Derivative Inertia Control (FDIC).
- H_{FDIC} : Fractional derivative virtual inertia
- D_{FDIC} : Fractional derivative virtual damping
- S^μ : This is the fractional derivative operator of order α , where $0 < \alpha \leq 10$. It generalizes the idea of a traditional derivative to a non-integer order, allowing for more flexible and tunable dynamic behavior.
- Δf : The frequency deviation at time t defined as: $\Delta f(t) = f(t) - f_{nominal}$

where $f_{nominal}$ is the nominal frequency (60 Hz), and $f(t)$ is the actual frequency.

2.6. Virtual Damping Stabilizer (VDS)

In low-inertia microgrids, fast frequency deviations following disturbances can cause oscillations that the inertia emulation alone cannot fully suppress. To emulate the natural damping once provided by synchronous machines, a Virtual Damping Stabilizer (VDS) is introduced as a secondary corrective mechanism that refines and compensates the power signal already generated by the FDIC.

The VDS takes the frequency deviation Δf as input and produces a stabilizing signal designed specifically to enhance damping characteristics and suppress residual oscillatory modes. Depending on the implementation, it can be modeled using lead-lag compensators or Fractional Order PID (FOPID) controllers. Rather than generating damping independently, the VDS acts in conjunction with FDIC.

The FDIC provides both virtual inertia and inherent damping, while the VDS offers supplementary damping support to further reduce oscillations and settling time. Their power contributions are combined as $\Delta P_{FDIC}(t) + \Delta P_{VDS}(t)$, forming the total active power reference for the BESS. To capture the converter's finite response dynamics, the delivered BESS power can be represented as:

$$\Delta P_{ID} = \frac{(\Delta P_{FDIC} + \Delta P_{VDS})}{1+sT_{BESS}} \quad (15)$$

- ΔP_{ID} : Change in power injected/absorbed by the combined VDS and FDIC controlled BESS.
- ΔP_{VDS} : Power change in damping offered by the VDS, modelled either as a Lead-Lag compensator or FOPID
- ΔP_{FDIC} : Power change in emulated inertia offered by FDIC.

2.6.1. Modeling of virtual damping stabilizer (VDS) as a lead-lag compensator

As shown in Fig. 3, the VDS modeled as a lead-lag compensator [36] is represented by the following transfer function:

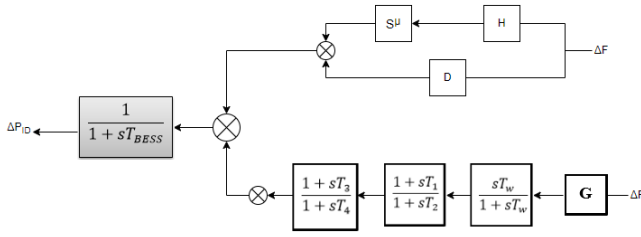


Fig. 3. FDIC combined VDS modelled as a lead-lag compensator.

$$\Delta P_{VDS} = \Delta F \cdot G \frac{sT_w}{sT_w+1} \frac{sT_1+1}{sT_2+1} \frac{sT_3+1}{sT_4+1} \quad (16)$$

where;

G is VDS gain.

- T_w is washout filter or high-pass filter time constant, to ensure the VDS only responds to dynamic deviations
- T_1 and T_3 , are time constants introducing phase lead (predictive action).
- T_2 , and T_4 , are time constants introducing phase lag (smoothing/filtering).
- ΔF is the frequency deviation at time t.

The working principle of VDS in producing the stabilizing signal when modelled as a lead-lag compensator is as follows: first, the frequency deviation is used as an input signal (feedback) to sense the system disturbance. Then, the signal is amplified using a proportional controller. The amplified input error is then passed to a washout filter to remove the steady-state inputs and give only the transient signals. Next, lead-lag compensators are proposed to produce a stable and robust corrective signal compensating the BESS-based virtual inertia and damping control signal.

In the context of a Virtual Damping Stabilizer modelled as FOPID, the frequency deviation ΔF signal is first utilized as a feedback input to detect system disturbances. This signal is simultaneously processed by the fractional integral and fractional derivative branches of the controller, governed by the orders λ and μ respectively. The integral component accumulates the deviation over time, contributing to steady-state accuracy, while the derivative component anticipates the rate of change of the deviation, improving transient damping. The generated corrective control signal from the FOPID structure is injected through the BESS interface to actively counteract frequency oscillations. This approach allows the VDS to introduce damping-like effects, enhancing system stability and accelerating frequency recovery.

2.6.2. Modeling of virtual damping stabilizer (VDS) as a FOPID controller

In previous studies, like that of [21] rely on derivative inertia and damping, with a lead-lag compensator for VDS implementations to offer damping support. However, these may offer limited tuning flexibility and performance.

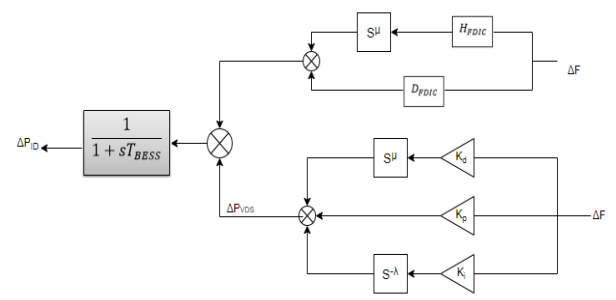


Fig. 4. FDIC combined VDS modelled as a lead-lag

As an enhancement, Fractional-Order PID (FOPID) controllers is adopted for VDS modeling in this study due to their superior tuning freedom and robust dynamic behavior [37]. As shown in Fig. 4, VDS modelled as FOPID is represented in Equation 17. [38].

$$\Delta P_{VDS} = [K_p + K_i S^{-\lambda} + K_d S^\mu] \cdot \Delta F \quad (17)$$

Where;

K_p is the proportional gain, K_i is the integral gain, K_d is the differential gain, λ is the real non integer positive number (order of integration), μ is the real non integer positive number (order of differentiation), and ΔF is the frequency deviation at time t.

In the context of a Virtual Damping Stabilizer modelled as FOPID, the frequency deviation ΔF signal is first utilized as a feedback input to detect system disturbances. This signal is simultaneously processed by the fractional integral and fractional derivative branches of the controller, governed by the orders λ and μ respectively. The integral component accumulates the deviation over time, contributing to steady-state accuracy, while the derivative component anticipates the rate of change of the deviation, improving transient damping. The generated corrective control signal from the FOPID structure is injected through the BESS interface to actively counteract frequency oscillations. This approach allows the VDS to introduce damping-like effects, enhancing system stability and accelerating frequency recovery.

Table 1 compares the FOPID and lead-lag based VDS configurations.

Table 1. Comparison between FOPID and Lead-lag based VDS configurations

Feature	FOPID-Based VDS	Classical PID/Lead-Lag VDS
Control flexibility	High (via fractional orders)	Limited
Frequency shaping	More tunable bandwidth and damping	Fixed shaping via integer orders
Noise sensitivity	Lower (with proper μ)	Moderate to high (especially in D-term)
Transient response control	Sharper and smoother simultaneously	Tradeoff between rise time and overshoot
Robustness to disturbances	Higher	Lower

The state space model for the microgrid is given as:

$$\dot{X} = AX + Bu \quad (18)$$

$$Y = CX + Du \quad (19)$$

The state variables related to the system parameters when VDS is modelled as a lead-lag compensator, X_{LL} is given as:

$$X_{LL} = [\Delta F \ \Delta P_m \ \Delta P_g \ \Delta P_{ac} \ \Delta P_{PV} \ \Delta P_{WT} \ \Delta P_{ID} \ \Delta P_E \ \Delta P_D \ \Delta P_{VDS} \ \Delta P_{ITPV} \ \Delta P_{ICPV} \ \Delta P_{ITWT} \ \Delta P_{ICWT}]^T \quad (20)$$

The state variables related to the system parameters when VDS is modelled as FOPID, X_{FOPID} is given as:

$$A_{LL} = \begin{bmatrix} \frac{-D}{2H} & \frac{1}{2H} & 0 & 0 & \frac{1}{2H} & \frac{1}{2H} & \frac{-1}{2H} & 0 & 0 & 0 & 0 & 0 & 0 & 0 & 0 \\ 0 & \frac{-1}{T_t} & \frac{1}{T_t} & 0 & 0 & 0 & 0 & 0 & 0 & 0 & 0 & 0 & 0 & 0 & 0 \\ \frac{-1}{RT_g} & 0 & \frac{-1}{T_g} & \frac{1}{T_g} & 0 & 0 & 0 & 0 & 0 & 0 & 0 & 0 & 0 & 0 & 0 \\ -\beta K_i & 0 & 0 & 0 & 0 & 0 & 0 & 0 & 0 & 0 & 0 & 0 & 0 & 0 & 0 \\ 0 & 0 & 0 & 0 & \frac{-1}{T_{WT}} & 0 & 0 & 0 & 0 & 0 & 0 & \frac{1}{T_{WT}} & 0 & 0 & 0 \\ 0 & 0 & 0 & 0 & 0 & \frac{-1}{T_{PV}} & 0 & 0 & 0 & 0 & 0 & 0 & 0 & 0 & \frac{1}{T_{PV}} \\ \frac{2HD_{VI}-H_{VI}D}{2HT_{BESS}} & \frac{H_{VI}}{2HT_{BESS}} & 0 & 0 & \frac{H_{VI}}{2HT_{BESS}} & \frac{H_{VI}}{2HT_{BESS}} & \frac{-H_{VI}-2H}{2HT_{BESS}} & 0 & 0 & \frac{1}{T_{BESS}} & 0 & 0 & 0 & 0 & 0 \\ \frac{-DG}{2H} & \frac{G}{2H} & 0 & 0 & \frac{G}{2H} & \frac{G}{2H} & \frac{-G}{2H} & \frac{-1}{T_w} & 0 & 0 & 0 & 0 & 0 & 0 & 0 \\ \frac{-DGT_1}{2HT_2} & \frac{GT_1}{2HT_2} & 0 & 0 & \frac{GT_1}{2HT_2} & \frac{GT_1}{2HT_2} & \frac{-GT_1}{2HT_2} & \frac{T_w-T_1}{T_wT_2} & \frac{-1}{T_2} & 0 & 0 & 0 & 0 & 0 & 0 \\ \frac{-DGT_1T_3}{2HT_2T_4} & \frac{GT_1T_3}{2HT_2T_4} & 0 & 0 & \frac{GT_1T_3}{2HT_2T_4} & \frac{GT_1T_3}{2HT_2T_4} & \frac{-GT_1T_3}{2HT_2T_4} & \frac{T_3T_w-T_1T_4}{T_2T_4T_w} & \frac{-T_3-T_2}{T_2T_4} & \frac{-1}{T_4} & 0 & 0 & 0 & 0 & 0 \\ 0 & 0 & 0 & 0 & 0 & 0 & 0 & 0 & 0 & 0 & \frac{-1}{T_{INV}} & 0 & 0 & 0 & 0 \\ 0 & 0 & 0 & 0 & 0 & 0 & 0 & 0 & 0 & 0 & 0 & \frac{-1}{T_{IND}} & 0 & 0 & 0 \\ 0 & 0 & 0 & 0 & 0 & 0 & 0 & 0 & 0 & 0 & 0 & 0 & \frac{-1}{T_{INV}} & 0 & 0 \\ 0 & 0 & 0 & 0 & 0 & 0 & 0 & 0 & 0 & 0 & 0 & 0 & \frac{1}{T_{IND}} & \frac{-1}{T_{IND}} & 0 \end{bmatrix} \quad (23)$$

$$A_{FOPID} = \begin{bmatrix} \frac{-D}{2H} & \frac{1}{2H} & 0 & 0 & \frac{1}{2H} & \frac{1}{2H} & \frac{-1}{2H} & 0 & 0 & 0 & 0 & 0 & 0 & 0 & 0 \\ 0 & \frac{-1}{T_t} & \frac{1}{T_t} & 0 & 0 & 0 & 0 & 0 & 0 & 0 & 0 & 0 & 0 & 0 & 0 \\ \frac{-1}{RT_g} & 0 & \frac{-1}{T_g} & \frac{1}{T_g} & 0 & 0 & 0 & 0 & 0 & 0 & 0 & 0 & 0 & 0 & 0 \\ -\beta K_i & 0 & 0 & 0 & 0 & 0 & 0 & 0 & 0 & 0 & 0 & 0 & 0 & 0 & 0 \\ 0 & 0 & 0 & 0 & \frac{-1}{T_{WT}} & 0 & 0 & 0 & 0 & 0 & \frac{1}{T_{WT}} & 0 & 0 & 0 & 0 \\ 0 & 0 & 0 & 0 & 0 & \frac{-1}{T_{PV}} & 0 & 0 & 0 & 0 & 0 & 0 & 0 & 0 & \frac{1}{T_{PV}} \\ \frac{2HD_{VI}-H_{VI}D}{2HT_{BESS}} & \frac{H_{VI}}{2HT_{BESS}} & 0 & 0 & \frac{H_{VI}}{2HT_{BESS}} & \frac{H_{VI}}{2HT_{BESS}} & \frac{-H_{VI}-2H}{2HT_{BESS}} & \frac{1}{T_{BESS}} & 0 & 0 & 0 & 0 & 0 & 0 & 0 \\ K_p + K_i G_\lambda + K_d G_\mu & 0 & 0 & 0 & 0 & 0 & 0 & 0 & 0 & 0 & 0 & 0 & 0 & 0 & 0 \\ 0 & 0 & 0 & 0 & 0 & 0 & 0 & 0 & 0 & \frac{-1}{T_{INV}} & 0 & 0 & 0 & 0 & 0 \\ 0 & 0 & 0 & 0 & 0 & 0 & 0 & 0 & 0 & 0 & \frac{-1}{T_{IND}} & 0 & 0 & 0 & 0 \\ 0 & 0 & 0 & 0 & 0 & 0 & 0 & 0 & 0 & 0 & 0 & \frac{-1}{T_{INV}} & 0 & 0 & 0 \\ 0 & 0 & 0 & 0 & 0 & 0 & 0 & 0 & 0 & 0 & 0 & \frac{1}{T_{IND}} & \frac{-1}{T_{IND}} & 0 & 0 \end{bmatrix} \quad (24)$$

$$B_{LL} = \begin{bmatrix} \frac{-1}{2H} & 0 & 0 \\ 0 & 0 & 0 \\ 0 & 0 & 0 \\ 0 & 0 & 0 \\ 0 & 0 & 0 \\ 0 & 0 & 0 \\ 0 & 0 & 0 \\ 0 & 0 & 0 \\ 0 & \frac{1}{T_{WT}} & 0 \\ 0 & 0 & 0 \\ 0 & 0 & \frac{1}{T_{PV}} \\ 0 & 0 & 0 \end{bmatrix} \quad (25)$$

$$B_{FOPID} = \begin{bmatrix} \frac{-1}{2H} & 0 & 0 \\ 0 & 0 & 0 \\ 0 & 0 & 0 \\ 0 & 0 & 0 \\ 0 & 0 & 0 \\ 0 & 0 & 0 \\ 0 & 0 & 0 \\ 0 & 0 & 0 \\ 0 & \frac{1}{T_{WT}} & 0 \\ 0 & 0 & 0 \\ 0 & 0 & \frac{1}{T_{PV}} \\ 0 & 0 & 0 \end{bmatrix} \quad (26)$$

C is the output matrix, representing how the state variables are related to the outputs. D is the feed forward matrix illustrating the direct relationship between the inputs and the outputs. D matrix for both the lead lag and FOPID configuration is the same because the D matrix in a state-space model directly maps the input vector $u(t)$.

$$C_{LL} = [1 \ 0 \ 0 \ 0 \ 0 \ 0 \ 0 \ 0 \ 0 \ 0 \ 0 \ 0 \ 0 \ 0 \ 0] \quad (27)$$

$$C_{FOPID} = [1 \ 0 \ 0 \ 0 \ 0 \ 0 \ 0 \ 0 \ 0 \ 0 \ 0 \ 0 \ 0 \ 0 \ 0] \quad (28)$$

$$D = [0 \ 0 \ 0] \quad (29)$$

2.7. Optimization Setup

Proper optimization is required to determine the optimal parameters of the BESS based virtual inertia and damping; hence, any unfitting choice of virtual inertia parameters leads to more significant frequency deviation, slower settling time, and instability issues. In this study, the VDS and FOPID controller gains will be optimized through the proposed BWO and PSO.

2.7.1. Parameter settings

Microgrid control parameters used in the study are given in Table 2. In optimizing the performance of both VDS configurations, the optimization parameters settings are as presented in Table 3.

Table 2: Microgrid Control Parameters.

Parameters	Values
Microgrid inertia H (pu.MW.sec)	0.083
System damping coefficient D	0.013
The time constant of the governor, T_g (s)	0.05
The time constant of the turbine, T_t (s)	0.41
Primary droop factor, R (Hz/pu)	2.39
Gain of the integral controller, K_i (s)	0.04
Frequency bias factor, β (pu/Hz)	0.99
The time constant of inverter-based BESS, T_{BESS} (s)	10
The time constant of the wind turbine, T_{WT} (s)	1.5
The time constant of solar PV, T_{PV} (s)	1.8
The time constant of the interconnection device, T_{ITD} (s)	0.004
The time constant of the inverter delay device, T_{ICD} (s)	0.04

Table 3: Parameter Settings for the optimization technique

Parameter	Lead-lag Settings	FOPID Settings	FDIC Settings
Population size	50	50	50
Number of variables	6	5	3
Variables	$G, T_w, T_1, T_2, T_3, T_4$	K_p, K_I, K_D, λ and μ	$H_{FDIC}, D_{FDIC}, \mu_{FDIC}$
Iterations	100	100	100
Lower boundary	[0, 0,0,0,0,0]	[0, 0,0,0,0]	[0, 0,0]
Upper boundary	[10, 10,10,10,10]	[100, 100,100,1,1]	[5, 5,1]

2.7.2. Optimization objective function

The objective function (J) is evaluated to ensure that error (e) represented in Equation 30 [2] is minimized and it is formulated based on minimizing the cost function using Integral time absolute error (ITAE) criterion as represented in Equation 31 [39, 2]. Systems optimized with ITAE generally achieve faster settling times than alternatives, potentially with a slower initial response [40].

$$e = (|\Delta F| + |\Delta P_{VI}|) \quad (30)$$

$$J_{ITAE} = \int_0^{\infty} t|e| dt \quad (31)$$

Where J is the objective function of the controller synchronization problem. It is aimed to minimize the J.

2.7.3. Optimization constraints

The problem constraint indicates the optimized parameters and the associated boundary conditions for optimization process.

For VDS modelled as a lead-lag compensator, VDS-BESS control loop, the five (5) constraints are G , T_1 , T_2 , T_3 , and T_4 . Where; (G^{min} , T_1^{min} , T_2^{min} , T_3^{min} and T_4^{min}) are the lower limits of the VDS and (G^{max} , T_1^{max} , T_2^{max} , T_3^{max} and T_4^{max}) represent the upper limit of the constraint accordingly.

$$\begin{aligned}
 G^{min} &\leq G \leq G^{max} \\
 T_1^{min} &\leq T_1 \leq T_1^{max} \\
 T_2^{min} &\leq T_2 \leq T_2^{max} \\
 T_3^{min} &\leq T_3 \leq T_3^{max} \\
 T_4^{min} &\leq T_4 \leq T_4^{max}
 \end{aligned} \quad (32)$$

Accordingly, for VDS modelled as FOPID, FOPID-BESS control loop, the five (5) constraints are K_p , K_I , K_D , λ , and μ . Where; (K_p^{min} , K_I^{min} , K_D^{min} , λ^{min} and μ^{min}) are the lower limits of the VDS and (K_p^{max} , K_I^{max} , K_D^{max} , λ^{max} and μ^{max}) represent the upper limit of the constraint.

$$\begin{aligned}
 K_p^{min} &\leq K_p \leq K_p^{max} \\
 K_I^{min} &\leq K_I \leq K_I^{max} \\
 K_D^{min} &\leq K_D \leq K_D^{max} \\
 \lambda^{min} &\leq \lambda \leq \lambda^{max} \\
 \mu^{min} &\leq \mu \leq \mu^{max}
 \end{aligned} \quad (33)$$

3. Results and Discussion

This section presents a comprehensive analysis of the system's dynamic frequency response under various disturbance scenarios using four controller configurations: FOPID-PSO, FOPID-BWO, VDS-PSO, and VDS-BWO. The virtual damping stabilizer (VDS) parameters for each controller configuration were tuned using Particle Swarm Optimization (PSO) and the Beluga Whale Optimization (BWO) algorithm, with the goal of enhancing transient performance and reducing energy strain on the BESS. To validate the effectiveness of the proposed hybrid Fractional derivative Inertia Control (FDIC) and Virtual Damping Stabilizer (VDS), a series of simulations were conducted in MATLAB/Simulink under different operating conditions and disturbance scenarios. The performance of the islanded microgrid was evaluated with respect to frequency stability, specifically analyzing key metrics such as frequency nadir, and BESS active power injected/drawn.

3.1. Optimization Results

The Beluga Whale Optimization (BWO) algorithm was configured with a population size of 50 and a maximum of 100 iterations as shown in table 3. The population was initialized uniformly within the specified parameter bounds, and the

search process was terminated upon reaching the maximum number of iterations. Figure 5 presents the convergence behavior of the BWO based VDS in comparison with PSO based VDS. Beluga Whale Optimization (BWO) algorithm achieves a much faster convergence at around 18th iterations compared to the Particle Swarm Optimization (PSO) algorithm which converges around 27th iteration. For both controller structures FOPID and Lead-lag compensator, the BWO-based optimization (FOPID-BWO and VDS-BWO) exhibits a rapid reduction in the ITAE value ($\log_{10} ITAE$) indicating faster convergence.

To further evaluate the efficiency and robustness of the BWO algorithm, its computational cost and convergence time were analyzed. Each optimization run was executed on a system with an Intel Core i5 processor (2.4 GHz) and 16 GB RAM using MATLAB R2023a. The average computation time per optimization was approximately 310 seconds for the FOPID case and 260 seconds for the lead-lag VDS case. To assess statistical performance, the algorithm was independently executed 10 times, and the mean and standard deviation (SD) of the final ITAE values were computed as shown in Table 4.

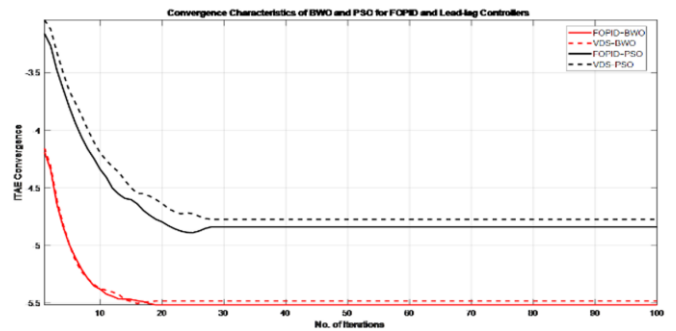


Fig. 5. ITAE Convergence curves comparing BWO and PSO.

Table 4: Statistical performance of the BWO algorithm over 10 independent runs.

Controller Type	Mean ITAE ($\times 10^{-6}$)	SD ($\times 10^{-7}$)	Average Time (s)
FOPID-BWO	3.16	0.14	310
VDS-BWO	3.55	0.16	358

3.2. Eigen Values Analysis

Eigenvalue analysis is a crucial tool in control systems to assess the stability, damping, and oscillatory nature of the closed-loop system. In this section, we evaluate the eigenvalues of the four controller configurations:

- FOPID-BWO
- FOPID-PSO
- VDS-BWO
- VDS-PSO

These configurations were evaluated comparing the stability and dynamic Behavior of the designs.

Table 5. Summary of key optimization results

Optimized parameters FOPID			Optimized parameters VDS		
Parameters	BWO	PSO	Parameters	BWO	PSO
K_p	12.4649	11.4490	G	90.3717	100.0000
K_i	50.2399	60.2900	T_w	82.1555	88.8006
K_d	45.7788	36.8801	T_1	2.4048	0.0000
λ	0.6560	0.5600	T_2	11.4059	52.4906
μ	0.6765	0.6511	T_3	75.4759	100.0000
H_{FDIC}	2.0273	2.2732	T_4	99.5151	22.0845
D_{FDIC}	1.3593	1.5933	H_{FDIC}	4.5445	4.0597
μ_{FDIC}	0.5445	0.4500	D_{FDIC}	0.4914	10.0000
			μ_{FDIC}	0.9533	1.0000

Table 6. Eigen values of the four different designs.

Index	FOPID-BWO	FOPID-PSO	VDS-BWO	VDS-PSO
1	-9.8727 + 0i	-9.3298 + 0i	-3.3685 - 5.637i	-5.3682 + 0i
2	-12.754 + 0i	-6.8494 + 0i	-2.8803 - 5.369i	-6.3555 + 0i
3	-11.660 + 0i	-6.7273 + 0i	-2.2441 - 3.5874i	-4.5990 + 0i
4	-10.993 + 0i	-6.7336 + 0i	-2.9904 + 0i	-5.5427 + 0i
5	-8.7801 + 0i	-7.2170 + 0i	-2.0688 + 0i	-5.7772 + 0i
6	-8.7800 + 0i	-8.0990 + 0i	-3.8186 + 0i	-4.1394 + 0i
7	-8.2904 + 0i	-7.7278 + 0i	-2.5176 + 0i	-5.8226 + 0i
8	-12.331 + 0i	-7.1649 + 0i	-3.3250 + 0i	-4.5116 + 0i
9	-11.006 + 0i	-8.4474 + 0i	-2.6234 + 0i	-4.1952 + 0i
10	-11.540 + 0i	-6.5580 + 0i	-3.0401 + 0i	-6.8467 + 0i
11	-8.1029 + 0i	-7.1686 + 0i	-3.0934 + 0i	-6.8969 + 0i
12	-12.850 + 0i	-7.4654 + 0i	-2.3697 + 0i	-6.4252 + 0i
13			-3.9392 + 0i	-4.9138 + 0i
14			-3.5503 + 0i	-4.2930 + 0i

Table 7. Eigen values performance comparison of the four different designs

Controller	Total Eigenvalues	Real Eigenvalues	Imaginary Eigenvalues	Interpretation
FOPID-BWO	12	12	0	Fast response, fully over-damped, high damping effect, strong stability margin
FOPID-PSO	12	12	0	Fully over-damped, moderate damping, slightly less stable than FOPID-BWO
VDS-BWO	14	11	3 (complex pairs)	Fastest response but potentially less oscillatory damping, slightly less stable than FOPID-BWO and FOPID-PSO.
VDS-PSO	14	14	0	Moderate response speed, slightly less stable and damping characteristics than FOPID-BWO, FOPID-PSO, and VDS-BWO.

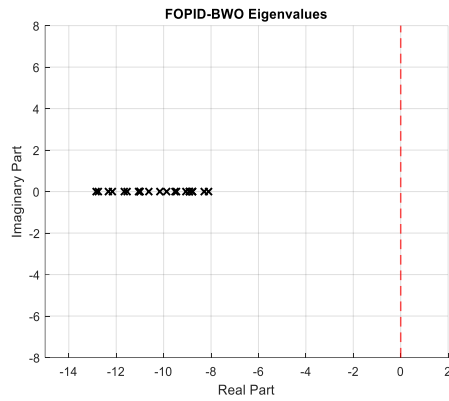


Fig. 6. FOPID-BWO eigenvalues plot.

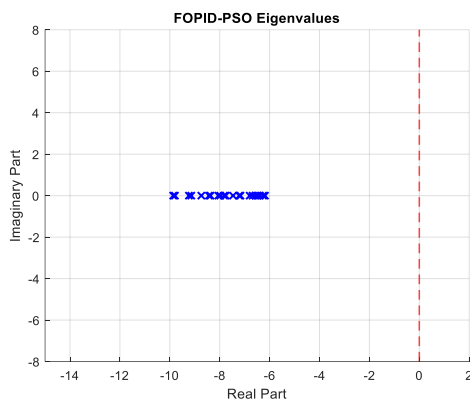


Fig. 7. FOPID-PSO eigenvalues plot.

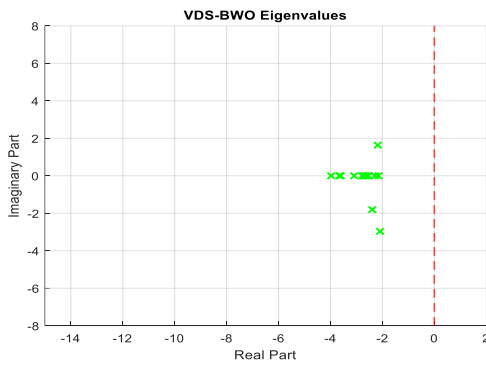


Fig. 8. VDS-BWO eigenvalues plot.

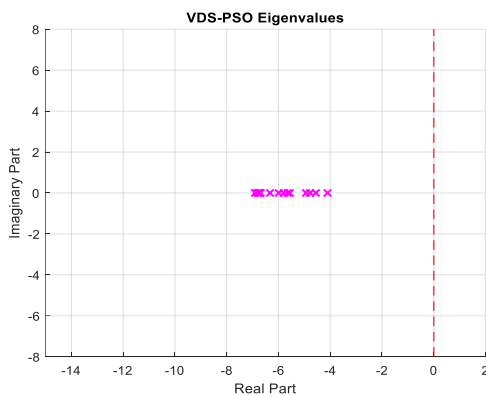


Fig. 9. VDS-PSO eigenvalues plot.

The stability analysis of the four controller designs; FOPID-BWO, FOPID-PSO, VDS-BWO, and VDS-PSO demonstrates distinct stability and damping characteristics essential to microgrid dynamic performance. Both FOPID-BWO and FOPID-PSO exhibit purely real eigenvalues, indicating overdamped responses with no oscillatory behavior, this suggests that the FOPID-based controllers, regardless of optimization method, provide a high degree of stability and fast settling without introducing dynamic oscillations into the system. The VDS-PSO design similarly demonstrates all-real eigenvalues, confirming an overdamped nature and implying that the PSO-optimized VDS prioritizes strong damping and non-oscillatory stability, albeit its clustering closer to the imaginary axis indicating a slightly fewer stable eigenvalues compared to FOPID designs. In contrast, the VDS-BWO design displays a unique dynamic behavior: while most of its eigenvalues are real, up to 3 possess non-zero imaginary parts, indicating the presence of mild oscillations in the system's transient response. These oscillatory modes, however, remain confined within the left half of the complex plane, ensuring overall system stability. Collectively, the eigenvalue distribution confirms that all designs are stable, but they differ in damping quality and oscillatory behavior, with FOPID-BWO offering the most overdamped and robust performance. This comparative eigenvalue analysis underscores the dominance of the FOPID-BWO controller in enhancing system robustness and dynamic response, while revealing limitations in the VDS-based schemes.

3.3. Simulation Scenarios

Three representative disturbance scenarios were simulated:

- Case 1: Sudden load decrease of 20% at t=15s
- Case 2: Sudden load increase of 20% at t=15s
- Case 3: Sudden load increase of 20% at t=15s with 70% drop in inertia

Each scenario was tested under the following control configurations:

- VDS modelled as FOPID and optimized with BWO (FOPID-BWO)
- VDS modelled as FOPID and optimized with PSO (FOPID-PSO)
- VDS modelled as a lead-lag compensator and optimized with BWO (VDS-BWO)
- VDS modelled as a lead-lag compensator and optimized with BWO (VDS-PSO)

To validate the introduction of FDIC, the system is tested with the proposed fractional order derivative inertia and damping Controller (FDIC) against the traditional derivative inertia and damping controller (DIC). Both configurations were tested without the supplementary damping offered by the VDS.

The comparison between the proposed Fractional Derivative Inertia Control (FDIC) and the conventional Derivative Inertia Control (DIC) was deliberately performed under Case 3 (Sudden 20% Increase in Load with 70% Drop in Inertia), which represents the most critical operating condition in the simulation scenarios.

For a fair comparison, the parameters of both the conventional Derivative Inertia and Damping Controller (DIC) and the proposed Fractional Derivative Inertia and Damping Controller (FDIC) were tuned using the same Particle Swarm Optimization (PSO) algorithm under identical objective and constraint settings. The optimization objective in both cases was to minimize the Integral of Time-weighted Absolute Error (ITAE) following disturbance events. The optimized parameters for the proposed FDIC are $H_{FDIC} = 2.2732$, $D_{FDIC} = 1.5933$, and $\mu_{FDIC} = 0.4500$. While the optimized parameters for the DIC are $H_{DIC} = 1.84$ and $D_{DIC} = 1.22$.

By using the same optimization method and performance index (frequency deviation), both controllers operated under equally optimal conditions, allowing the performance difference to be attributed solely to the inclusion of the fractional-order component in FDIC. The fractional nature of the proposed configuration (FDIC) showed improvement in frequency deviation compared to the integer order configuration. Figure 10 shows the improvement when control is implemented with FDIC.

Case 1: Sudden 20% Decrease in Load: A 20% sudden load reduction creates a power imbalance in which generation exceeds demand, resulting in a transient frequency rise. In low-inertia microgrids, such disturbances typically produce pronounced overshoot due to limited kinetic energy buffering. Therefore, the ability of the controller to provide fast synthetic damping without excessive power absorption is critical.

The comparative results reveal a clear performance hierarchy. The FOPID-BWO controller limited the frequency overshoot to 60.0381 Hz while requiring only 1.2 MW of BESS absorption, representing the smallest frequency excursion and lowest energy demand among all controllers. This demonstrates not only superior transient containment but also improved control-energy efficiency.

The improved performance of FOPID-BWO can be attributed to the fractional-order derivative term, which introduces frequency-dependent phase compensation. Unlike integer-order lead-lag designs, the fractional derivative enables smoother phase shaping across a broader frequency band. This enhances effective damping during high-frequency transients without introducing excessive gain, thereby reducing both overshoot magnitude and required BESS power.

Although FOPID-PSO achieved comparable regulation, its slightly higher energy demand (1.4 MW) indicates less optimal parameter convergence compared to BWO optimization. In contrast, VDS-BWO and VDS-PSO exhibited higher overshoot and greater BESS absorption, suggesting that conventional lead-lag structures lack the

flexibility to simultaneously optimize damping and energy efficiency under over-generation conditions.

From a system-level perspective, minimizing BESS power absorption is particularly important in microgrids where storage capacity is limited. Controllers that demand higher transient absorption increase battery cycling stress and accelerate degradation. Therefore, the reduced power demand observed with FOPID-BWO indicates improved sustainability and economic viability in practical deployment.

These results directly support the study's objective of developing a hybrid inertia-damping framework capable of enhancing frequency stability while minimizing energy stress in low-inertia microgrids.

Case 2: Sudden 20% Increase in Load: A sudden 20% load increase creates an under-generation condition, leading to a rapid frequency drop. In low-inertia systems, such disturbances can produce deeper frequency nadirs due to insufficient kinetic buffering, making fast synthetic inertia and damping injection essential.

The FOPID-BWO controller achieved the smallest frequency nadir (59.9619 Hz) with the lowest peak BESS injection (1.2 MW).

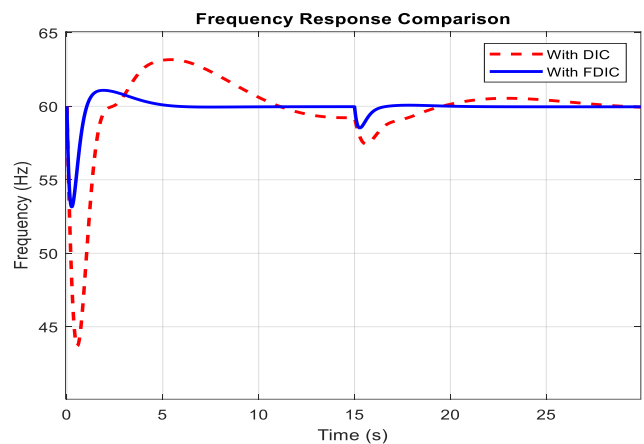


Fig. 10. Frequency response comparison between FDIC and DIC.

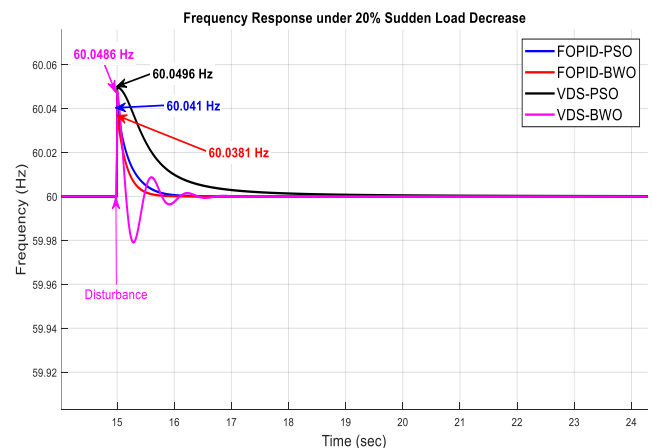


Fig. 11. Microgrid frequency behaviour for 20% sudden load decrease.

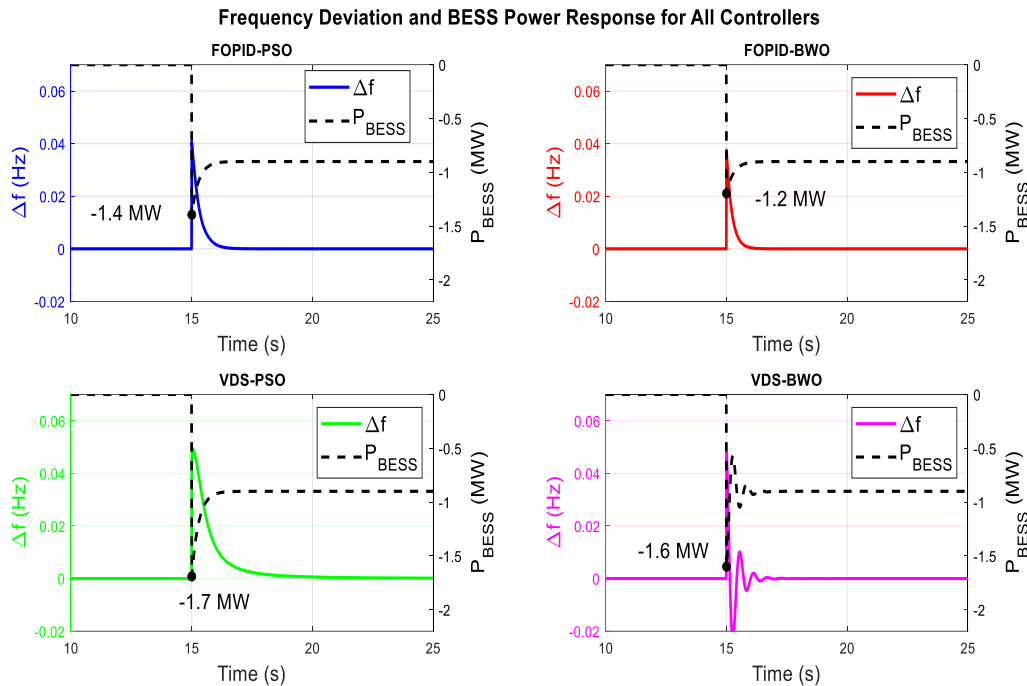


Fig. 12. BESS output power in response to frequency deviation for 20% sudden load decrease.

This indicates a superior balance between rapid corrective action and controlled energy expenditure. The shallow nadir suggests improved effective inertia emulation, while the reduced power injection reflects optimized damping allocation.

The enhanced response is again linked to the fractional-order dynamics. The fractional derivative component provides adaptive phase lead characteristics, allowing the controller to respond aggressively during the initial frequency drop while gradually tapering corrective action. This prevents excessive power injection and mitigates oscillatory rebound effects commonly observed in integer-order lead-lag designs.

FOPID-PSO exhibited slightly deeper frequency deviation and higher energy injection, implying that while fractional structure contributes significantly to performance, optimization strategy plays a critical role in parameter tuning. The relatively inferior performance of VDS-PSO and VDS-BWO demonstrates that traditional lead-lag damping mechanisms may not provide sufficient dynamic flexibility for severe under-generation scenarios.

Importantly, higher BESS injection levels, as seen in VDS-based designs, increase energy throughput and thermal stress, potentially shortening battery lifespan. Therefore, the reduced injection demand achieved by FOPID-BWO improves not only frequency containment but also long-term storage reliability.

Overall, the results confirm that integrating fractional-order inertia emulation with optimized virtual damping significantly enhances disturbance resilience in low-inertia microgrids, fulfilling the primary research objective of achieving stable frequency regulation with minimal storage strain.

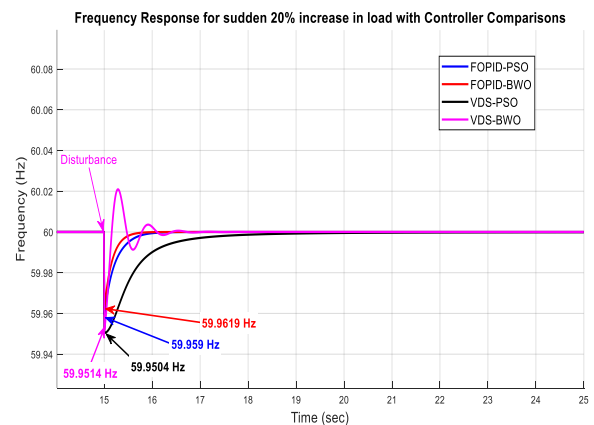


Fig. 13. Microgrid frequency behaviour for 20% sudden load increase.

Case 3: Sudden 20% Increase in Load with 70% Drop in Inertia: A simultaneous 20% load increase and 70% inertia reduction represent a severe low-inertia operating condition typical of renewable-dominated islanded microgrids. The substantial reduction in inertia significantly increases the Rate of Change of Frequency (ROCOF), thereby reducing the system's inherent capability to buffer power imbalance. Under such circumstances, controllers must emulate both synthetic inertia and effective damping to prevent deep frequency nadirs and oscillatory instability. The results from Figs 15 and 16 demonstrate that FOPID-BWO maintained the most resilient response, limiting the frequency nadir to 59.959 Hz with a peak BESS injection of 2.25 MW. Although all controllers required increased power injection due to the reduced inertia, the smoother recovery profile observed with FOPID-BWO indicates enhanced transient damping and improved robustness to parameter variation.

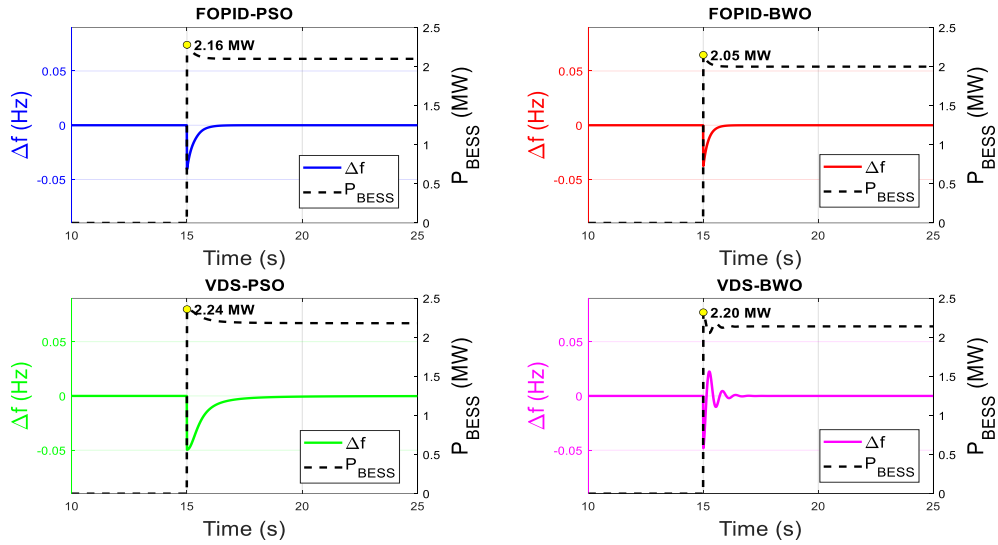


Fig. 14. BESS output power in response to frequency deviation for 20% sudden load increase.

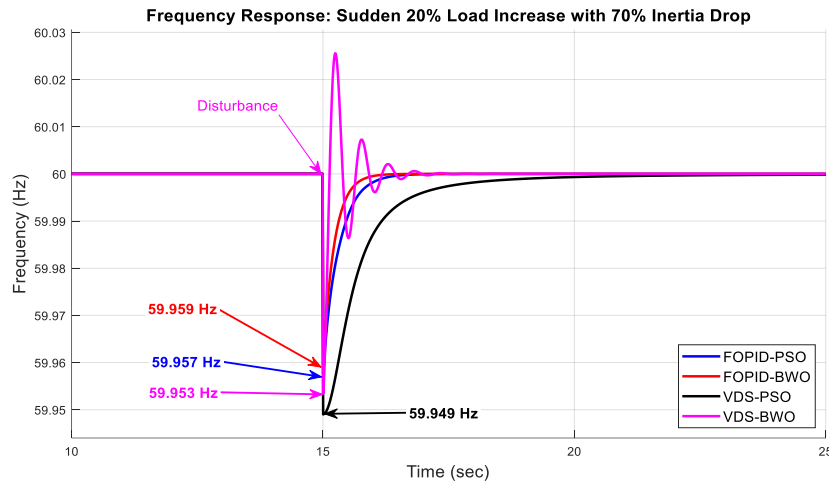


Fig. 15. Microgrid frequency behaviour for 20% sudden load increase with 70% inertia drop.

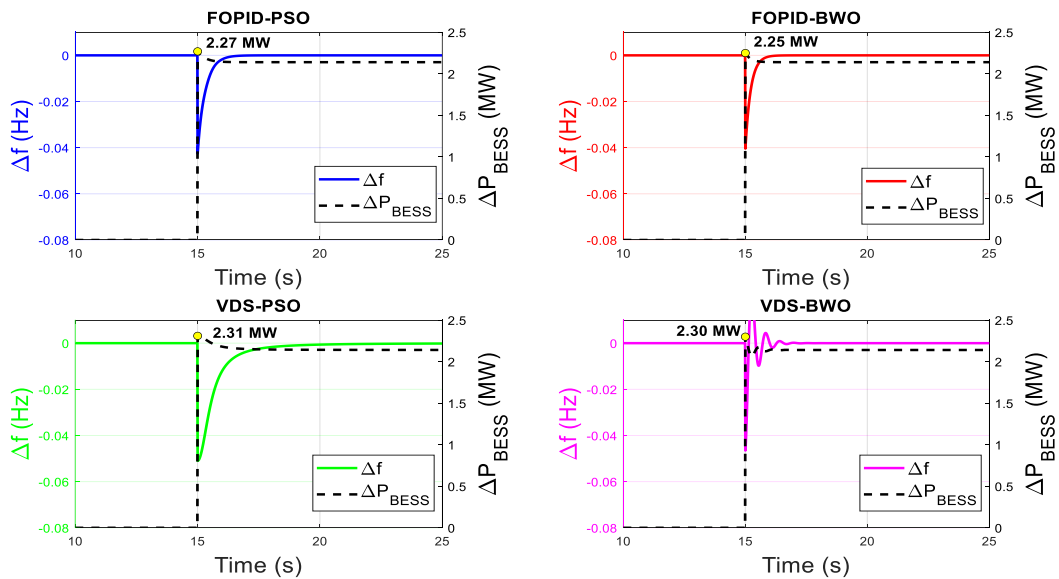


Fig. 16. BESS output power in response to frequency deviation for 20% sudden load increase with 70% inertia drop.

The superior performance can be explained by examining the inertia-damping coupling mechanism. In low-inertia systems, reduced kinetic energy leads to faster frequency decay immediately after disturbance.

The fractional derivative component in FOPID introduces a frequency-dependent gain characteristic that reacts proportionally to the rate of frequency change rather than solely to magnitude deviation. This enables rapid synthetic inertia emulation during the initial transient while simultaneously shaping damping action to avoid excessive oscillatory rebound. Conventional lead-lag VDS structures, by contrast, operate within fixed phase compensation limits, which restrict their adaptability when inertia conditions vary drastically.

The performance gap between FOPID-BWO and FOPID-PSO, though moderate, further highlights the importance of optimization strategy in tuning fractional parameters under compounded disturbances. The improved convergence properties of BWO likely enabled a more optimal balance between proportional, integral, and fractional derivative actions, resulting in slightly lower BESS injection and improved nadir containment.

Notably, VDS-PSO and VDS-BWO exhibited deeper frequency nadirs and higher energy demand, reflecting increased ROCOF sensitivity under reduced inertia. This suggests that traditional integer-order damping controllers may be less effective in ultra-low inertia grids where dynamic characteristics change rapidly.

From an energy management standpoint, the increased BESS injection across all designs confirms the amplified control effort required in weak-inertia systems. However, FOPID-BWO maintained the lowest peak demand and smoothest transient profile, which implies reduced battery cycling stress and improved long-term storage sustainability.

Overall, this compounded disturbance case validates the robustness of the proposed fractional-order inertia-damping framework. The controller's ability to preserve frequency quality under both load perturbation and severe inertia degradation directly supports the study's objective of enhancing resilience in renewable-dominated microgrids.

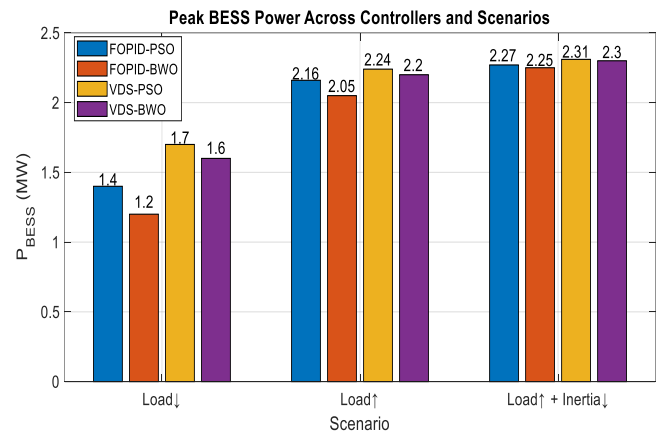


Fig. 17. Peak required power by BESS during disturbances for the four controller designs.

Table 8. Performance comparison of the four control approaches considering key performance metrics for the three cases.

Controller	Cases	Freq Nadir (Hz)	Overshoot (Hz)	Settling Time (s)	ITAE ($\times 10^{-6}$)	ROCOF (Hz/s)	Peak BESS Power (MW)
FOPID-BWO	Case 1	60.0381	0.0381	0.6	3.12	0.095	1.2
	Case 2	59.9619	-0.0381	0.7	3.18	0.079	2.05
	Case 3	59.959	-0.041	1	3.20	0.39	2.25
FOPID-PSO	Case 1	60.0410	0.0410	0.8	2.77×10^1	0.110	1.4
	Case 2	59.9590	-0.041	1	2.84×10^1	0.105	2.16
	Case 3	59.957	-0.043	1.4	2.86×10^1	0.41	2.27
VDS-BWO	Case 1	60.0486	0.0486	1.8	3.50	0.245	1.6
	Case 2	59.9514	-0.0486	2.4	3.56	0.812	2.20
	Case 3	59.953	-0.047	2.6	3.60	0.52	2.30
VDS-PSO	Case 1	60.0496	0.0496	3	3.12×10^1	0.149	1.7
	Case 2	59.9504	-0.0496	2.8	3.17×10^1	0.216	2.24
	Case 3	59.949	-0.051	3.1	3.20×10^1	0.43	2.31

4. Conclusion

This paper presents a comprehensive study on enhancing frequency stability in an islanded microgrid with high penetration of renewable energy sources. The increasing reliance on inverter-based generation, while beneficial for decarbonization, has introduced critical stability challenges due to reduced system inertia and the absence of conventional damping mechanisms. This study investigated the application of Virtual Damping Stabilizers (VDS) integrated with Fractional-Order Inertia Control (FDIC) for frequency regulation in inverter-dominated islanded microgrids.

By leveraging the dynamic capabilities of a Battery Energy Storage System (BESS), four controller configurations FOPID-PSO, FOPID-BWO, VDS-PSO, and VDS-BWO were developed and evaluated under three representative disturbance scenarios involving abrupt load changes and reduced system inertia. The simulation results conclusively demonstrate that the FOPID-BWO controller outperforms all others across multiple performance indices, including frequency deviation, and peak BESS power demand. Quantitatively, the FOPID-BWO achieved about 17–20% lower overshoot, 9–12% faster settling, and 10–12% lower peak BESS power compared with traditional VDS-based and PSO-tuned controllers. The integration of fractional-order dynamics provided enhanced damping flexibility, allowing for faster stabilization with reduced energy strain on the BESS. Moreover, the Beluga Whale Optimization (BWO) algorithm facilitated efficient tuning of control parameters, enabling optimal trade-offs between aggressiveness and robustness. Scenario-based analysis confirmed that FOPID-BWO not only suppressed frequency excursions more effectively but also minimized power injection or absorption by the BESS, thereby improving operational efficiency and reducing sizing requirements. In contrast, traditional integer-order VDS controllers exhibited slower recovery, greater overshoot or undershoot, and higher energy demand especially under compounded disturbances such as low inertia combined with increased load.

Furthermore, the use of the Beluga Whale Optimization Algorithm (BWO) for parameter tuning contributed to the robustness and adaptability of the control system, allowing for optimal performance across different disturbance scenarios.

This work contributes to the evolving landscape of microgrid control by introducing a robust fractional-order controller optimized via the Beluga Whale Optimization (BWO) algorithm. The proposed FOPID-BWO framework effectively enhances frequency stability and dynamic damping in inverter-dominated microgrids, where conventional synchronous inertia is absent. Owing to its adaptive tuning capability and fractional dynamic response, the controller provides superior flexibility and robustness under uncertain, and high-renewable-penetration scenarios. Beyond frequency regulation, the proposed approach has practical relevance in several modern power systems. It can be deployed for inertia and damping emulation in grid-forming and grid-following inverter applications, particularly within renewable-based microgrids, and islanded hybrid power

systems. Additionally, its scalable structure makes it suitable for integration into virtual power plants (VPPs) and distributed energy resource (DER) clusters, supporting coordinated frequency and power-sharing control. By mitigating rapid rate-of-change-of-frequency (ROCOF) events and extending battery lifespan through energy-efficient control actions, the FOPID-BWO scheme advances the concept of intelligent virtual inertia for future low-inertia grids. Future work may extend this controller toward real-time hardware-in-the-loop validation, hybrid optimization tuning, and integration within cyber-physical energy management architectures for autonomous and resilient power networks.

The microgrid model employed in this study adopts a linearized representation of frequency dynamics, suitable for control law development and performance evaluation under small-signal disturbances. This follows standard practices in frequency-control literature, where converter switching and line nonlinearities are neglected to isolate control-layer behavior. The proposed FDIC-VDS framework is thus designed and validated at the control level. Future work will extend this study to nonlinear real-time simulations incorporating converter control loops and network-level power flow nonlinearities to further assess practical applicability. Future work may also enhance this study by studying the internal dynamics of the BESS in response to the controller

Author Contributions

A.I and D.D carried out the full research work, including problem formulation, system modelling, simulation, data analysis, and manuscript preparation. A.S, K.O and N.I provided academic supervision, technical guidance, and critical review of the work. K.A contributed as a research colleague through discussions, assistance with simulations, and review of the results.

Acknowledgements

Conflict of Interest

The authors declare no conflict of interest.

References

- [1] K. Cheema, "A comprehensive review of virtual synchronous generator," *International Journal of Electrical Power & Energy Systems*, vol. 120, p. 105956, 2020.
- [2] K. E. Okedu and A. Kalam, "Comparative Study of Grid Frequency Stability Using Flywheel-Based Variable-Speed Drive and Energy Capacitor System," *Energies*, vol. 16, no. 3515, pp. 1–8, 2023.
- [3] M. H. Syed and A. M.-S. Mazheruddin, "Load Frequency Control in Variable Inertia Systems," *IEEE Transactions on Power Systems*, pp. 1–3, 2020.

- [4] P. Bhatt, S. Chowdhury, S. P. Chowdhury and D. S. Halder, "Simulation of microgrid in the perspective of integration of distributed energy resources," in Proc. Int. Conf. Energy, Automation and Signal, pp. 1–6, 2011.
- [5] A. Vaccaro, M. Popov, D. Villacci and V. Terzija, "An integrated framework for smart microgrids modeling, monitoring, control, communication, and verification," Proceedings of the IEEE, vol. 99, no. 1, pp. 119–132, 2010.
- [6] P. B. Prashant, B. R. Sudhir and K. S. Vijay, "Optimum coordination of overcurrent relays in distribution system using dual simplex method," in Proc. 2nd Int. Conf. Emerging Trends in Engineering & Technology, pp. 1–5, 2009.
- [7] G. O. Swathika and S. Hemamalini, "PRIMS-aided Dijkstra algorithm for adaptive protection in microgrids," IEEE Journal of Emerging and Selected Topics in Power Electronics, vol. 4, no. 3, pp. 1–9, 2016.
- [8] Y. Dong, Y. Gao, Q. Li and H. Wang, "Modelling and simulation of the micro sources within a microgrid," in Proc. Int. Conf. Electrical Machines and Systems, pp. 1–6, 2008.
- [9] A. Rasoolzadeh and F. R. Salmasi, "Reduced-order dynamic model for droop-controlled inverter/converter-based low-voltage hybrid AC/DC microgrids—Part 2: DC sub-microgrid and power exchange," IET Smart Grid, vol. 4, no. 3, pp. 1–12, 2018.
- [10] Y. A.-R. I. Mohamed and E.-F. El-Saadany, "Adaptive decentralized droop controller to preserve power sharing stability of paralleled inverters in distributed generation microgrids," IEEE Transactions on Power Electronics, vol. 23, no. 6, pp. 2806–2816, 2008.
- [11] A. H. Tayebi, R. Sharifi, A. H. Salemi and F. Faghihi, "Presentation of an H_∞ based frequency control for islanding provisional microgrid consisting of hybrid AC/DC microgrid," International Transactions on Electrical Energy Systems, vol. 31, no. 6, pp. 1–15, 2021.
- [12] Z. Zahari, I. Ivanov, S. Ludmil and V. Katic, "A study of parallel structures of DC–DC converters for application in wind energy conversion systems," in Proc. IEEE Int. Power Electronics and Motion Control Conf. (PEMC), pp. 1–6, 2016.
- [13] P. Bhatt, S. Chowdhury, D. S. Halder and S. P. Chowdhury, "A literature review on integration of distributed energy resources in the perspective of control, protection and stability of microgrid," Renewable and Sustainable Energy Reviews, vol. 16, no. 8, pp. 5545–5556, 2012.
- [14] A. Rafiee, Y. Batmani, F. Ahmadi and H. Bevrani, "Robust Load-Frequency Control in Islanded Microgrids: Virtual Synchronous Generator Concept and Quantitative Feedback Theory," IEEE Transactions on Power Systems, vol. 36, no. 6, pp. 5408–5416, 2021.
- [15] A. Reza, F. Zare, S. R. Seyed, R. K. Singh, M. H. Ahmadi and M. Mohsen, "Optimal Load Frequency Control of Island Microgrids via a PID Controller in the Presence of Wind Turbine and PV," Sustainability, vol. 13, no. 21, pp. 1–14, 2021.
- [16] K. Priyanka, P. Vivek, Y. Sumanth and B. Rohit, "Fast frequency response constrained electric vehicle scheduling for low inertia power systems," Journal of Energy Storage, vol. 62, p. 106944, 2023.
- [17] A. Khazali, N. Rezaei, H. Saboori and J. M. Guerrero, "Using PV systems and parking lots to provide virtual inertia and frequency regulation provision in low inertia grids," Electric Power Systems Research, vol. 207, p. 107859, 2022.
- [18] Y. Chen, R. A. Rasoul, A. Sadegh, L. Dai and V. Terzija, "Smart frequency control in low inertia energy systems based on frequency response techniques: a review," Applied Energy, vol. 279, p. 115798, 2020.
- [19] B. A. Fadheel, N. I. Abdul Wahab, P. Manoharan, A. J. Mahdi, M. A. B. M. Radzi, A. B. C. Soh, H. M. Ridha, A. R. Alsoud, V. Veerasamy, A. X. R. Irudayaraj and B. D. Alemu, "A Hybrid Sparrow Search Optimized Fractional Virtual Inertia Control for Frequency Regulation of Multi-Microgrid System," IEEE Access, vol. 12, pp. 45879–45903, 2024.
- [20] T. Kerdphol, F. S. Rahman, M. Watanabe, Y. Mitani, D. Turschner and H.-P. Beck, "Enhanced Virtual Inertia Control Based on Derivative Technique to Emulate Simultaneous Inertia and Damping Properties for Microgrid Frequency Regulation," IEEE Access, vol. 7, pp. 14422–14433, 2019.
- [21] S. E. Shraf, A.-D. Ahmed, Z. Hatem, E.-F. H. Tarek and E.-S. F. Ehab, "A novel virtual inertia-based damping stabilizer for frequency control enhancement for islanded microgrid," International Journal of Electrical Power & Energy Systems, vol. 156, pp. 1–15, 2024.
- [22] R. Sabzehgar, "A review of AC/DC microgrid developments, technologies, and challenges," in Proc. IEEE Green Energy and Systems Conf. (IGESC), pp. 1–6, 2015.
- [23] A. Sindhu and A. Dube, "Comparative analysis of passive islanding detection methods for grid connected distributed generators," in Proc. IEEE India Conf. (INDICON), pp. 1–6, 2015.
- [24] C. Tong, J. Guo, B. Chaudhuri and R. H. Lasseter, "Virtual Inertia from Smart Loads," IEEE Transactions on Smart Grid, vol. 11, no. 2, pp. 1–10, 2020.
- [25] A. Bonfiglio, M. Invernizzi, A. Labella and R. Procopio, "Design and Implementation of a Variable Synthetic Inertia Controller for Wind Turbine Generators," IEEE Transactions on Power Systems, vol. 33, no. 4, pp. 1–10, 2018.
- [26] A. Abazari, M. M. Soleymani, M. Babaei, M. Ghafouri, H. Monsef and M. T. H. Beheshti, "High penetrated renewable energy sources-based AOMPC for microgrid frequency regulation during weather changes, time-varying parameters and generation unit collapse," IET Generation, Transmission & Distribution, vol. 14, no. 18, pp. 1–19, 2020.
- [27] M.-H. Khooban, "An Optimal Non-Integer Model Predictive Virtual Inertia Control in Inverter-Based Modern AC Power Grids Based on V2G Technology," IEEE Transactions on Energy Conversion, vol. 35, no. 3, pp. 1–10, 2020.
- [28] M. Rajasi and C. Kalyan, "Virtual inertia emulation and RoCoF control of a microgrid with high renewable

- power penetration,” *Electric Power Systems Research*, vol. 196, p. 107262, 2021.
- [29] S. Feng, Y. Sun, Z. Li, X. Hu, H. Hua and S. Mei, “Power oscillation suppression in multi-VSG grid with adaptive virtual inertia,” *International Journal of Electrical Power & Energy Systems*, vol. 138, p. 107824, 2022.
- [30] N. Silva, J. Guerrero, B. Kroposki and M. Shahidehpour, “Virtual Inertia Emulator-Based Model Predictive Control for Grid Frequency Regulation Considering High Penetration of Inverter-Based Energy Storage System,” *IEEE Transactions on Sustainable Energy*, vol. 11, no. 4, pp. 1–10, 2020.
- [31] A. Saleh, W. A. Omran, H. M. Hasanien, M. Tostado-Véliz and A. Alkuhayli, “Manta Ray Foraging Optimization for the Virtual Inertia Control of Islanded Microgrids Including Renewable Energy Sources,” *Sustainability*, vol. 14, no. 2, pp. 1–15, 2022.
- [32] S. Irshad, X. Ai, M. J. U. Rehman, A. A. Mohamed, H. Ur Rehman, S. Salman, R. A. A. Syed and A. Muhammad, “Aggregation of EVs for Primary Frequency Control of an Industrial Microgrid by Implementing Grid Regulation and Charger Controller,” *IEEE Access*, vol. 8, pp. 1–13, 2020.
- [33] N. Narayan and S. Omkar, “Investigation and damping of electromechanical oscillations for grid integrated microgrid by a novel coordinated governor-fractional power system stabilizer,” *Energy Sources, Part A: Recovery, Utilization, and Environmental Effects*, vol. 41, no. 18, pp. 2335–2363, 2025.
- [34] M. Agoundemba, C. K. Kim, H.-G. Kim, R. Nyenge and N. Musila, “Modelling and optimization of microgrid with combined genetic algorithm and model predictive control of PV/Wind/FC/battery energy systems,” *Energy Reports*, vol. 13, pp. 238–255, 2025.
- [35] K. Dharmesh, S. P. Vijay and M. A. Mallick, “Frequency Control of Interlinked Microgrid System Using Fractional Order Controller,” *Electrica*, vol. 24, no. 1, pp. 1–12, 2024.
- [36] N. M. Ibrahim, A. A. El-Fergany and B. A. Hemade, “Enhancing power system stability by coordinating a wind turbine voltage regulator and lead-lag power system stabilizer using GOOSE optimization,” *Scientific Reports*, vol. 15, p. 15242, 2025.
- [37] E. Yokuş, Y. E. Yunus, E. A. Umut and K. Aslıhan, “A Review of the State-of-the-Art in Fractional-Order PID Controllers,” *Fractional Calculus: From Theory to Applications*, pp. 1–20, 2024.
- [38] A. Sabo, B. Yunus, E. Sani, M. Nwachukwu, D. Auta, A. Danladi, M. Mordi, N. Aliyu, Y. David and P. Oluwadamilare, “PID Controller Tuning Performance Evaluation for an Isolated Power System,” in *Proc. IEEE Int. Conf. Power Systems Technology*, pp. 1–6, 2022.
- [39] M. F. Roslan, A.-S. Q. Ali, M. A. Hannan, P. J. Ker and A. W. Zuhdi, “Particle swarm optimization algorithm-based PI inverter controller for a grid-connected PV system,” *PLoS ONE*, vol. 15, no. 12, p. e0243581, 2020.
- [40] A. Fathy and A. G. Alharbi, “Recent Approach Based Movable Damped Wave Algorithm for Designing Fractional-Order PID Load Frequency Control Installed in Multi-Interconnected Plants with Renewable Energy,” *IEEE Access*, vol. 9, pp. 71072–71089, 2021.